Parallel evolution of two clades of a major Atlantic endemic *Vibrio parahaemolyticus* pathogen lineage by independent acquisition of related pathogenicity islands

Feng Xu[1,2,3], Narjol Gonzalez-Escalona[4], Kevin P. Drees[1,2], Robert P. Sebra[5], Vaughn S. Cooper[1,2,*], Stephen H. Jones[1,6], and Cheryl A. Whistler[1,2#]

Running Title: parallel evolution of ST631 *Vibrio parahaemolyticus*

[1]Northeast Center for Vibrio Disease and Ecology, University of New Hampshire, Durham, NH; [2]Department of Molecular, Cellular and Biomedical Sciences, University of New Hampshire, Durham, NH; [3]Genetics Graduate Program, University of New Hampshire, Durham, NH; [4]Center for Food Safety and Applied Nutrition, Food and Drug Administration, College Park, MD; [5]Icahn Institute and Department of Genetics & Genomic Sciences, Icahn School of Medicine at Mount Sinai, New York, NY; and [6]Department of Natural Resources and the Environment, University of New Hampshire, Durham, NH, USA.

*Current address: Microbiology and Molecular Genetics, University of Pittsburgh School of Medicine, Pittsburgh, PA

#Corresponding author e-mail: cheryl.whistler@unh.edu

ABSTRACT

Shellfish-transmitted *Vibrio parahaemolyticus* infections have recently increased from locations with historically low disease incidence, such as the Northeast United States (US). This change coincided with a bacterial population shift towards human pathogenic variants occurring in part through the introduction of several Pacific native lineages (ST36, ST43 and ST636) to near-shore areas off the Atlantic coast of the Northeast US. Concomitantly, ST631 emerged as a major endemic pathogen. Phylogenetic trees of clinical and environmental isolates indicated that two clades diverged from a common ST631 ancestor, and in each of these clades, a human pathogenic variant evolved independently through acquisition of distinct *Vibrio* pathogenicity islands (VPaI). These VPaI differ from each other and bear little resemblance to hemolysin-containing VPaI from isolates of the pandemic clonal complex. Clade I ST631 isolates either harbored no hemolysins, or contained a chromosome I-inserted island we call VPaIβ that encodes a type three secretion system (T3SS2β) typical of Trh hemolysin-producers. The more clinically prevalent and clonal ST631 clade II had an island we call VPaIγ that encodes both *tdh* and *trh* and that was inserted in chromosome II. VPaIγ was derived from VPaIβ but with some additional acquired elements in common with VPaI carried by pandemic isolates, exemplifying the mosaic nature of pathogenicity islands. Genomics comparisons and amplicon assays identified VPaIγ-type islands containing *tdh* inserted adjacent to the *ure* cluster in the three introduced Pacific and most other emergent lineages. that collectively cause 67% of Northeast US infections as of 2016.

IMPORTANCE

The availability of three different hemolysin genotypes in the ST631 lineage provided a unique opportunity to employ genome comparisons to further our understanding of the processes underlying pathogen evolution. The fact that two different pathogenic clades arose in parallel from the same potentially benign lineage by independent VPaI acquisition is surprising considering the historically low prevalence of community members harboring VPaI in waters along the Northeast US Coast that could serve as the source of this material. This illustrates a possible predisposition of some lineages to not only acquire foreign DNA but also to become human pathogens. Whereas the underlying cause for the expansion of *V. parahaemolyticus* lineages harboring VPaIγ along the US Atlantic coast and spread of this element to multiple lineages that underlies disease emergence is not known, this work underscores the need to define the environment factors that favor bacteria harboring VPaI in locations of emergent disease.

INTRODUCTION

Vibrio parahaemolyticus is an emergent pathogen capable of causing human gastric infections when consumed, most often with contaminated shellfish (1, 2). Some human pathogenic *V. parahaemolyticus* variants evolve from diverse non-pathogenic communities through horizontal acquisition of *Vibrio* pathogenicity islands (VPaI) (3-5). Gastric pathogenic *V. parahaemolyticus* typically harbor islands with at least one of two types of horizontally acquired hemolysin genes (*tdh* and *trh*) that are routinely used for pathogen discrimination even though their role in disease appears modest (6-11). Most pathogenic *V. parahaemolyticus* isolates also carry accessory type three secretion systems (T3SS) that translocate effector proteins that contribute to host interaction (12-14). Two evolutionarily divergent horizontally-acquired accessory systems (T3SS2α or T3SS2β) contribute to human disease and are genetically linked

66 to hemolysin genes (two *tdh* genes with T3SS2α, and *trh* with T3SS2β) in contiguous but distinct
67 islands (4, 15-17). The first described *tdh*-harboring island [called by several different names
68 including Vp-PAI (15), VPaI-7 (4), and *tdh*VPA (17)] from an Asian pandemic strain called
69 RIMD 2210366 is fairly well-characterized (4, 5, 13, 18, 19). In contrast, islands containing
70 T3SS2β linked to *trh* and a urease (*ure*) cluster, which confers a useful diagnostic phenotype,
71 [where similar islands are described by others as Vp-PAI$_{TH3966}$ (16), or *trh*VPA(17, 20)] have
72 received only modest attention. Pathogenic variants harboring both *tdh* and *trh* are increasingly
73 associated with disease in North America (21-26), and yet, to our knowledge, the exact
74 configuration of hemolysin-associated VPaI(s) in isolates that contain both *tdh* and *trh* have not
75 yet been described [although see (20)]. Thus it is unclear how virulence loci and islands in these
76 emergent pathogen lineages carrying both hemolysins evolved and spread.
77 The expanding populations of *V. parahaemolyticus* have increased infections even in
78 temperate regions previously only rarely impacted by this pathogen and where most
79 environmental isolates harbor no known virulence determinants (27). A related complex of Asia-
80 derived pandemic strains, most often identified as serotype O3:K6 and also known as sequence
81 type (ST) 3 (based on allele combinations of seven housekeeping genes) causes the most disease
82 globally (28). An unrelated Pacific native lineage called ST36 (also described as serotype
83 O4:K12) currently dominates infections in North America, including from the Northeast United
84 States (US) (21, 26, 29). The introduction of ST36 into the Atlantic Ocean by an unknown route
85 precipitated a series of outbreaks from Atlantic shellfish starting in 2012 (29, 30). Prior to 2012,
86 residential lineages contributed to low but increasing sporadic infection rates on the Northeast
87 US coast (https://www.cdc.gov/vibrio/surveillance.html, 2017) (21), with ST631 emerging as the
88 major lineage that is endemic to near-shore areas of the Atlantic Ocean bordering North America

(the northwest Atlantic Ocean) (31). However, we previously identified a single ST631 isolate lacking hemolysins (21, 27) suggesting this pathogen lineage may have recently evolved through VPaI acquisition.

The goal of our study was to understand the genetic events and changing population context for the evolution of the ST631 pathogenic lineage. We conducted whole and core genome phylogenetic analysis of three environmental and 39 clinical ST631 isolates along with isolates from other emergent lineages from the region, which revealed two ST631 clades of common ancestry, from which human pathogens evolved in parallel. The single clade I clinical isolate acquired a *recA* gene insertion previously seen associated with Asian lineages, and had a VPaI that is typical of isolates harboring *trh* in the absence of *tdh.* In contrast, isolates from the clonal ST631 clade II that dominates Atlantic-derived ST631 infections (31) had a related but distinct VPaI. This VPaI contained a *tdh* gene and four associated hypothetical protein encoding genes inserted within, not next to, an existing *ure-trh*-T3SS2β island in close proximity to the *ure* cluster. Nearly all emergent resident and invasive lineages, including all three Pacific lineages (ST36, ST636 and ST43) contained islands that similarly had a *tdh* gene inserted within the VPaI in an identical location adjacent to the *ure* cluster providing a mechanism for simultaneous acquisition of both hemolysins with T3SS2β.

RESULTS

Atlantic endemic ST631 and several invasive lineages harboring both the *tdh* and *trh* hemolysin genes are clinically prevalent in four reporting Northeast US States.

Ongoing analysis of clinical isolates revealed that even as the Pacific-derived ST36 lineage continued to dominate infections (50%), the endemic (autochthonous) ST631 lineage

accounted for 14% of infections (Table 1). Concurrently, a limited number of other lineages contributed individually to fewer infections (≤3% each), among which were two lineages that have caused infections in the Pacific Northwest in prior decades: ST43 and ST636 (22, 23). ST43 and ST636 only recently (2013 and 2011 respectively) (21) have been linked to product harvested from waters along the Northeast US coast, and also caused infections in subsequent years. As is common among US clinical isolates, pathogenic isolates of all the aforementioned lineages harbor both the *tdh* and *trh* hemolysin genes (Table 1). Among environmental isolates, ST34 and ST674 are the most frequently recovered pathogen lineages but these caused comparatively few infections (Table 1). ST34 was first reported from the environment in 1998, from both the Gulf of Mexico and near-shore areas of MA, and was also recovered in NH in 2012 (21) suggesting it is an established resident in the region. ST674 which was first reported from an infection in Virginia in 2007 (32) was first recovered from the local environment in 2012 (www.pubmlst.org/vparahaemolyticus) (21). Notably even though all four ST674 environmental isolates, like ST34, harbored both hemolysin genes, the single ST674 clinical isolate (MAVP-21) lacked hemolysins (Table 1) (21). The decrease in clinical prevalence of *trh*-harboring Atlantic endemic ST1127, which caused no infections in the last three years, coincided with the increase in clinical prevalence of all three Pacific-derived lineages which harbor both hemolysins. Notably, very few other clinical isolates harbored *trh* in the absence of *tdh* and clinical isolates containing only *tdh* (i.e. ST1725) were extremely rare (Table 1). Concurrent with this shift in composition of clinical lineages that includes multiple Pacific-derived lineages, hemolysin producers have increased in relative abundance in nearshore areas of the region, where historically these represented ~1% of all isolates (27). Since 2012, hemolysin producers have been recovered more frequently, and in the last two years their proportion has increased by

up to an order of magnitude (comprising as much as 10%) in some regional shellfish associated populations (data not shown).

A single clinical ST631 lineage isolate with an unusual *recA* allele harbors *trh* in the absence of *tdh*

Employing ST631-specific marker-based assays (see methods), we identified two additional 2015 environmental isolates (one from NH and one from MA) and one additional 2011 local-source clinical isolate (MAVP-R) (21) with a hemolysin profile (*trh*$^{+}$ without *tdh*) that is atypical of the ST631 lineage (Table 1). Although analysis of the seven-housekeeping gene allele combination confirmed the environmental isolates were indeed ST631, MAVP-R was not ST631 based on only one locus: *recA*. Examination of the *recA* locus of MAVP-R uncovered a large insertion within the ancestral ST631 *recA* gene (allele recA21; www.pubmlst.org/vparahemolyticus) incorporating an intact but different *recA* gene into the locus [allele recA107(33)] and fragmenting the ancestral gene (Fig. 1). The insertion in the ancestral *recA* gene in MAVP-R is identical to one observed in the *recA* locus of two Hong Kong isolates (isolates S130 and S134) and similar to the one in isolate 090-96 (ST189a) isolated in Peru but believed to have originated in Asia (33).

ST631 forms two divergent clades

The existence of three different hemolysin profiles (Table 1) among all available ST631 draft genomes suggested there could be more than one ST631 lineage. Therefore we evaluated whole genome maximum likelihood (ML) phylogenies of select ST631 isolates and all other lineages causing two or more infections reported in four Northeast US States to evaluate whether

158 there was more than one ST631 lineage (Table 1) (Fig. 2). The phylogenetic tree showed that
159 ST631 isolates, regardless of their hemolysin genotype, clustered together but they formed two
160 distinct clades, indicative of common ancestry (Fig. 2). Clade I harbored either *trh* or no
161 hemolysins and consisted of all three environmental isolates which were from MA and NH, and
162 the single clinical isolate MAVP-R, whereas clade II consisted of all other isolates all of which
163 harbor both hemolysins. The two distinct ST631 clades shared 85% of their DNA in common
164 and displayed polymorphisms in ≤12% of the shared DNA content. The most closely related
165 sister lineage to ST631 was formed by *trh*-harboring ST1127 isolates that have been exclusively
166 reported from clinical sources in the Northeast US (21).

167 We next evaluated the relationships of all available ST631 isolate genomes at NCBI and
168 sequenced by us (Supplemental Table 1) using a custom core genome multi-locus sequence
169 typing (cgMLST) method as previously described (31). Minimum spanning trees built from core
170 genome loci from 42 ST631 isolates indicated that only 390 loci varied between the most closely
171 related isolate of clade I (MAVP-L) and clade II (G6928) (Fig. 3). The most distantly related
172 isolates within clade I (G149 and MAVP-R) exhibited 80 core genome loci differences whereas
173 clade II is clonal with only 51 variant loci between the most divergent isolates: clinical isolate
174 09-4436 and environmental isolate S487-4, both reported from PEI Canada (Fig. 3) (31).
175
176 **Each ST631 clade independently acquired a distinct pathogenicity island positioned on**
177 **different chromosomes**

178 Given the variation in ST631, comparisons between these isolates could elucidate the
179 events that led not only to the evolution of two pathogenic clades but also address unresolved
180 questions about the unique configurations and contents of pathogenicity islands in western

Atlantic Ocean emergent lineages. The physical proximity of *tdh* with the *ure* cluster and *trh*, and the co-occurrence of *tdh* with T3SS2β reported in many tdh^+/trh^+ clinical isolates suggested *tdh* could be harbored within or next to the same pathogenicity island harboring *trh* in at least some lineages as was previously suggested (20, 24, 34).

To identify the location and determine the architecture of the pathogenicity elements harboring hemolysin genes, we generated high quality annotated genomes for the clade I ST631 isolate MAVP-R and clade II ST631 isolate MAVP-Q (both reported in 2011 from MA) employing PacBio sequencing. The pathogenicity island regions in these isolates genomes were extracted, aligned, and the contents compared with pathogenicity island harboring two *tdh* genes [previously called Vp-PAI (15), VPaI-7 (4) and *tdh*VPA(17)] from RIMD 2210366 and Vp-PAI_{TH3996} (16) [also called *trh*VPI (17)] harboring *trh* (Supplemental Table 2). This comparison revealed that MAVP-R harbored a pathogenicity island typical of *trh*-containing isolates that includes a linked *ure* cluster and T3SS2β that is orthologous, with the exception of few unique regions, with Vp-PAI_{TH3996} (16) (Supplemental Table 2 and Fig. 4). Because the lack of convention in uniformly naming syntenous islands that distinguish them from distinctive and yet functionally analogous islands can impede communication, we hereafter will consistently reference the same island by a common descriptive name regardless of isolate lineage. Hereafter we will refer to islands sharing the same general configuration to that in MAVP-R by the name VPaIβ, and refer to *tdh*-containing islands similar to that described in strain RIMD 2210366 by the name VPaIα, regardless of bacterial isolate background. We adopted this simplified nomenclature in reference to the version of the key virulence determinant carried in the islands (T3SS2α and T3SS2β) in the two already described island types. This scheme importantly accommodates naming of additional uniquely-configured islands as they are identified. As noted

204 previously (16, 17, 20), VPaIβ is dissimilar to VPaIα in most gene content with ~ 78 ORFs
205 unique to VPaIβ (where the number of identified ORFs used for comparison can differ slightly
206 depending on which annotation program is applied) (Supplemental Table 2, Fig. 4). Even so,
207 VPaIβ had many homologous genes of varying sequence identity (n=~38 ORFs, excluding *tdh*
208 homology with *trh*) when compared to VPaIα (Supplemental Table 2, Fig. 4)(4, 5, 16).
209 Identification of some homologs required that we relax matching to 50% such as for the
210 divergent, but homologous T3SS2α and T3SS2β genes encoding the apparatus, chaperones, and
211 some shared effectors (Supplemental Table 2). No homolog of the T3SS2α effector gene *vopZ*
212 was identified, but a single ORF whose deduced protein sequence bears only 27% identity with
213 VopZ is located in its place (Fig. 2 and Supplemental Table 2). VPaIβ from strain TH3996 and
214 VPaIα from pandemic strain RIMD 2210633 are inserted in an identical location in chromosome
215 II adjacent to an Acyl-CoA hydrolase-encoding gene. In contrast the VPaIβs in MAVP-R,
216 ST1127 isolate MAVP-25, and Asia-derived AQ4037 are in chromosome I, in each case in the
217 same insertion location identified for strain AQ4037 (17).
218 MAVP-Q contained both *tdh* and *trh* within the same contiguous unique VPaI (hereafter
219 called VPaIγ) that shared features with both VPaIα and VPaIβ (Fig. 4, Supplemental Table 2).
220 Specifically, VPaIγ had a core that with few exceptions was orthologous in content and
221 syntenous with VPaIβ from MAVP-R (Fig. 4) with only a few exceptions. VPaIγ displays high
222 conservation with VPaIα near its 3' end, as has been described in other draft $tdh^{+}trh^{+}$ harboring
223 genomes (20) as well as in the VPaIβ island of strain TH3996, although the presence of this
224 element may not be typical of VPaIβ (e.g. it is absent in the islands from AQ4037 (17), MAVP-
225 R and MAVP-25). The VPaIγ also contained a *tdh* gene homologous to *tdh2* (also called *tdhA*)
226 from VPaIα (98.6%) near its 5' end but not at the 5' terminus of the island (Fig. 4). Rather, the

DNA flanking both sides of the *tdh* gene in VPaIγ was conserved in VPaIβ of MAVP-R and absent from VPaIα, (Fig. 4). Analysis of 300 genomes of *V. parahaemolyticus* (representing a minimum of 28 distinct sequence types) of sufficient quality for analysis confirmed that the module of four hypothetical proteins preceding the *tdh2* homolog was present only in *trh*-harboring genomes, but not in genomes harboring *tdh* in the absence of *trh* (i.e. VPaIα containing genomes), providing evidence that the *tdh* gene was acquired horizontally by insertion into, not next to, an existing VPaIβ, perhaps through activity of the adjacent transposase gene (11) (Supplemental Table 3, Supplemental fig. 1, and data not shown). Like with VPaIα from RIMD 2210633, and VPaIβ of TH3996, VPaIγ of clade II ST631 is located in a conserved location of chromosome II, adjacent to an Acyl-CoA hydrolase-encoding gene.

The final environmental ST631 clade I isolate that lacked hemolysins, G149, had no VPaIα, β or γ elements in its genome. Close examination of the DNA corresponding to the VPaI insertion sites in either chromosome revealed no remnants of these islands in either chromosomal location indicating this isolate likely never acquired a pathogenicity island (Supplemental Fig. 2 and data not shown). Because clade I isolate G149 lacked these islands, this could be the ancestral state of the ST631 lineage (21).

Most clinically prevalent isolates from the Northeast US harbor similar contiguous pathogenicity islands containing *tdh* inserted in the same location of their VPaI

We next asked which isolates from other lineages likely residing within the mixed population with ST631 in near-shore areas of the Northeast US harbored islands of similar structure to VPaIγ that contain both hemolysin genes. Assembly of short-read sequences into contigs that cover the full length of VPaI which is necessary for comparative analysis of entire

island configuration was impeded by the fact that homologous transposase sequences and other sequences were repeated multiple times throughout the island. Therefore, we determine whether other lineages harboring both hemolysin genes harbor *tdh* in the same island location, between the conserved VPaIβ/γ module of four hypothetical proteins (to the left or 5' of *tdh*) and the *ure* cluster (to the right or 3' of *tdh*) (Fig. 4) by combining bioinformatics analysis of sequenced genomes with amplicon assays (Supplemental Fig. 1). First we analyzed assembled draft genomes for *tdh* co-occurrence and proximity with the four adjacent hypothetical protein-encoding genes that are absent in VPaIβ but present in VPaIγ (See Methods). Every emergent pathogenic lineage of the Northeast US (Table 1) harboring both *tdh* and *trh* carried homologous DNA corresponding to all four hypothetical proteins adjacent to the *tdh* gene in a contiguous segment (Supplemental Table 3). To determine whether *tdh* was also adjacent to the *ure* cluster in these same isolates we next designed specific flanking primers and amplified the unique juncture between the *tdh*-containing transposon associated module and the *ure* cluster for all clinical isolates harboring both *tdh* and *trh* (See Methods) (Supplemental Fig. 1). The results were congruent with our bioinformatics assessment (Supplemental Table 3), and demonstrated that isolates from all emergent pathogenic lineages harboring both hemolysins have *tdh* inserted in close proximity to an *ure* cluster in a configuration similar to VPaIγ from MAVP-Q (Fig. 5, Table 1). This confirmed that these isolates harboring both hemolysins harbor *tdh* within, and not next to, the same VPaI thereby facilitating simultaneous acquisition of both hemolysin genes.

DISCUSSION

Even preceding the increased illnesses from Pacific-invasive lineages, two different clades of the predominant endemic Atlantic lineage of pathogenic *V. parahaemolyticus*, ST631

(31) evolved and contributed to a rise in sporadic illnesses in the four reporting Northeast US States (Table 1, Fig. 2 & 3). Several lines of evidence support the interpretation of parallel pathogen evolution. The two lineages exhibit differences in both clinical and environmental prevalence suggesting the pathogenic variants of each clade have not evolved the same degree of virulence (Table 1). Pathogenic members in each lineage also acquired different pathogenicity islands with different hemolysin gene content (Fig. 2 & 3). Although it was a formal possibility that ST631 clade II evolved from clade I by independent horizontal acquisition of *tdh* into its existing VPaIβ, it is notable that other resident and even invasive lineages now in the Atlantic harbor VPaIγ with *tdh* and four additional co-occurring ORFs inserted into the same location of the island, suggesting a common evolutionary origin of this hybrid-type island (Fig. 4 and Supplemental Fig. 1). Finally, each of the two clades harbor VPaI insertions on different chromosomes: the less clinically prevalent ST631 clade I contains three isolates that harbor VPaIβ in chromosome I (Fig. 3) and a single environmental isolate lacking any island (Table 1, supplemental Fig. 2), whereas the clonal ST631 clade II isolates all harbor VPaIγ on chromosome II.

Given that several other resident lineages harbor similar β and γ-type VPaI, pathogens in each clade could have acquired their islands from the reservoir of resident bacteria already circulating in the Atlantic even before the presume arrival of invasive Pacific lineages. Several well-documented members of the Gulf of Mexico *V. parahaemolyticus* population (35-37) may also have expanded their range through movement of ocean currents and could be the source for these VPaI (Table 1, Fig. 5). But historically, hemolysin producers were extremely rare in near shore areas of the Atlantic US coast (25) and represented only about ~1% of isolates in an estuary of NH as of a decade ago (27) limiting the potential for interacting partners or sources for

296 acquired VPaI. Given this historical context, it is remarkable that two different clades from the
297 same lineage independently acquired different VPaI-which for clade II ST631 occurred prior to
298 2007 -well before the recent shift in abundance of hemolysin producers.
299 The parallel evolution of two different lineages through lateral DNA acquisition alludes
300 to the possibility that as-yet-undefined attributes may increase the chances of acquisition or
301 prime some bacterial lineages (such as ST631) to more readily acquire and maintain genetic
302 material or become pathogenic upon island acquisition. Even though the ecological niche in
303 which horizontal island acquisition took place is unknown, it is conceivable that co-colonization
304 of hosts or substrates favorable to the growth of ST631 and hemolysin producers may have
305 facilitated island movement. Certainly, association of bacteria with specific marine substrates
306 such as chitinous surfaces of plankton that also induce a natural state of competence could
307 promote lateral transfer through close contact between the progenitors of the pathogenic
308 subpopulation of each clade and island donors (3, 38, 39). Alternatively, conjugative plasmids or
309 transducing phage could have been the agents of island delivery. The finding that the only
310 clinical clade I isolate, MAVP-R, also harbors a second horizontal insertion in its *recA* locus that
311 matched one previously found in Asia-derived strains (33) indicates it acquired more than one
312 segment of foreign DNA during its evolution as a pathogen (Fig. 1) further illustrating that
313 mechanisms that facilitate DNA transfer and acquisition may both have been at play. It also
314 suggests that horizontal transfer of DNA from introduced bacteria not yet detected in the Atlantic
315 could add to the genetic material available for pathogen evolution from Atlantic Ocean
316 populations. The more detailed molecular epidemiological, comparative genomics, and
317 functional analyses necessary to assess the impact of introduced pathogens on resident Atlantic

lineages are warranted given this evidence and the documented introduction of multiple Pacific-derived lineages in the region (Table 1).

There has been some consideration of the roles of human virulence determinants in ecological fitness, but the natural context of pathogenic *V. parahaemolyticus* evolution is still unknown (40-42). Whereas *tdh* and T3SS2α each may promote growth when bacteria are under predation, isolates that carry *trh*-containing islands (which likely also have T3SS2β) do not derive similar benefits from their islands (43). This is surprising considering the islands encode several homologous effectors (Fig. 4 and Supplemental Table 2) that don't have an established role in enteric disease but they could alternatively or additionally mediate eukaryotic cell interactions with natural hosts thereby promoting environmental fitness (13, 14). But these islands also lack homologous open for the VPaIα effector that is most closely associated with enteric disease: *vopZ* (11) (Fig. 4 and Supplemental Table 2). The general lack of knowledge of unique T3SS2β effectors and other gene function in these islands (Fig. 4 and Supplemental Table 2) even with regard to enteric disease, limits comparative analysis with the well-studied and functionally defined VPaIα which could elucidate the bases for pathogen evolution. The higher clinical prevalence of clade II ST631 than clade I which has also been recovered on more than one occasion from the environment (Table 1) could indicate that VPaIγ confers greater virulence potential than VPaIβ, perhaps owing to the presence of *tdh*, a known virulence factor (1, 7, 44). However, the resident community members in both the Pacific and the Atlantic Ocean that harbor *tdh* and T3SS2α comparatively rarely cause human infections (21-23). The unique environmental conditions that underlie pathogen success from northern latitudes that favors bacteria with VPaIβ and VPaIγ including two different ST631 lineages suggests the shared content of these islands could confer abilities that are distinct from VPaIα which could underlie

341 the repeated acquisition and maintenance of these related islands by so many different lineages
342 now present in near-shore areas of the Northeast US.
343
344 **MATERIALS AND METHODS**
345 **Bacteria isolates, media and growth conditions.**
346 *V. parahaemolyticus* clinical isolates for this study were provided by cooperating public
347 health laboratories in Massachusetts, New Hampshire, Maine, and Connecticut whereas a select
348 number of environmental isolates were enriched from estuarine substrates as described (21).
349 Detailed information about these isolates was described previously (31) and listed in
350 Supplemental Table 1. Isolates were routinely cultured in Heart Infusion (HI) media
351 supplemented with NaCl at 37°C as described (21).
352
353 **Whole genome sequencing, assembly, annotation and sequence type identification.**
354 Genomic DNA was extracted using the Wizard Genomic DNA purification Kit (Promega,
355 Madison WI USA) or by organic extraction (21). The quality genomic DNA was determined by
356 spectrophotometric measurements by NanoDrop (ThermalFisher, Waltham MA USA). Libraries
357 for DNA sequencing were prepared using a high-throughput Nextera DNA preparation protocol
358 (45) using an optimal DNA concentration of 2ng/µl. Genomic DNA was sequenced using an
359 Illumina – HiSeq2500 device at the Hubbard Center for Genome Studies at the University of
360 New Hampshire, using a 150bp paired-end library. *De novo* assembly was performed using the
361 A5 pipeline (46), and the assemblies annotated with Prokka1.9 using the "genus" option and
362 selecting "*Vibrio*" for the reference database (47). The sequence types were subsequently
363 determined using the SRST2 pipeline (48). The sequence type of each genome was determined

364 when using *V. parahaemolyticus* as the database (https://pubmlst.org/vparahaemolyticus/). For
365 most isolates where the combination of each allele was not found in the database representing
366 novel sequence types, the genome was submitted for a new sequence type designation
367 (www.pubmlst.org/vparahaemolyticus).

368 Isolates MAVP-Q and MAVP-R were sequenced using the Pacific Biosciences RSII
369 technology. Using between 3.7-5.3 µg DNA, the library preparation and sequencing was
370 performed according to the manufacturer's instructions (Pacific Biosciences, Menlo Park CA,
371 USA) and reflects the P5-C3 sequencing enzyme and chemistry for MAVP-Q isolate and the P6-
372 C4 configuration for MAVP-R. The mass of double-stranded DNA was determined by Qubit
373 (Waltham, MA USA) and the sample diluted to a final concentration of 33 µg / µL in a volume
374 of 150 µL elution buffer (Qiagen, Germantown MD USA). The DNA was sheared for 60
375 seconds at 4500 rpm in a G-tube spin column (Covaris, Wobrun MA USA) which was
376 subsequently flipped and re-spun for another 60 seconds at 4500 rpm resulting in a ~20,000 bp
377 DNA verified using a DNA 12000 Bioanalyzer gel chip (Agilent, Santa Clara, CA USA). The
378 sheared DNA isolate was then re-purified using a 0.45X AMPure XP purification step (Beckman
379 Coulter, Indianapolis IN USA). The DNA was repaired by incubation in DNA Damage Repair
380 solution. The library was again purified using 0.45X Ampure XP and SMRTbell adapters ligated
381 to the ends of the DNA at 25ºC overnight. The library was treated with an exonuclease cocktail
382 (1.81 U/µL Exo III 18 and 0.18 U/µL Exo VII) at 37ºC for 1 hour to remove un-ligated DNA
383 fragments. Two additional 0.45X Ampure XP purifications steps were performed to remove
384 <2000 bp molecular weight DNA and organic contaminant.

385 Upon completion of library construction, samples were validated using an Agilent
386 DNA 12000 gel chip. The isolate library was subjected to additional size selection to the range

of 7,000 bp – 50,000 bp to remove any SMRTbells < 5,000 bp using Sage Science Blue Pippin 0.75% agarose cassettes to maximize the SMRTbell sub-read length for optimal *de novo* assembly. Size-selection was confirmed by Bio-Analysis and the mass was quantified using the Qubit assay. Primer was then annealed to the library (80ºC for 2 minute 30 followed by decreasing the temperature by 0.1º/s to 25ºC). The polymerase-template complex was then bound to the P5 or P6 enzyme using a ratio of 10:1 polymerase to SMRTbell at 0.5 nM for 4 hours at 30ºC and then held at 4ºC until ready for magbead loading, prior to sequencing. The magnetic bead-loading step was conducted at 4ºC for 60-minutes per manufacturer's guidelines. The magbead-loaded, polymerase-bound, SMRTbell libraries were placed onto the RSII machine at a sequencing concentration of 110-150 pM and configured for a 180-minute continuous sequencing run. Long read assemblies were constructed using HGAP version 2.3.0 for *de novo* assembly generation. Further, hybrid assemblies were generated and error corrected with illumina raw reads using Pilon v1.20 (49).

Lineage-specific marker-based assays

To more rapidly identify ST631 isolates from clinical and environmental collections we developed PCR-amplicon assays to unique gene content in ST631. Whole genome comparisons were performed on MAVP-Q (a ST631 clinical isolate), G149 (a ST631 environmental isolate), MAVP-26 (ST36), RIMD2210633 (ST3), and AQ4037 (ST96) (Supplemental Fig. 3). A total of 26 distinct genomic regions, each greater than 1kb in size, were present in MAVP-Q but absent in other comparator genomes, including environmental ST631 that lacks hemolysins (G149) (Supplemental Fig. 3). Within a large genomic island ~37.6 Kb in length with an integrase at one terminus and an overall lower GC content (40.6% compared to 45.8% for the genome) a single

ORF homologous to restriction endonucleases (AB831_06355) that was restricted to clinical ST631 isolates in our collection and publicly available draft genomes (n=693) (http://www.ncbi.nlm.nih.gov/genome/691, 2017) was selected as a suitable amplicon target. The distribution of this locus was further analyzed using the BLAST algorithm by a query against the nucleotide collection, the non-redundant protein sequences, and against the genus *Vibrio* (taxid: 662), excluding *V. parahaemolyticus* (taxid: 691), using the default settings for BLASTn (50). Similar approaches were applied to identify ST631 diagnostic loci inclusive of the single environmental isolate (G149), which identified a hypothetical protein encoding region (AB831_06535) (ST631env). Oligonucleotide primers were designed to amplify the diagnostic regions including AB831_06355 using primers ST631*end* F (5'AGTTCATCAGGTAGAGAGTTAGAGGA3') and ST631*end*R (5'TCTTCGTTACCATAGTATGAGCCA3') which produces and amplicon of c.a. 494bp, and AB831_06535 using primers ST631envF (5'TGGGCGTTAGGCTTTGC3') and ST631-envR (5'GGGCTTCTACGACTTTCTGCT3') producing an amplicon of 497bp.

Amplification of diagnostic loci was evaluated in individual assays using genomic DNA from positive and negative controls: MAVP-Q and G149 (ST631), G4186 (ST34), G3578 (ST674), and MAVP-M (ST1127), MAVP-26 (ST36) and G61 (ST1125). Amplification of specific sequence types were performed with Accustart enzyme mix on purified DNA. Cycling was performed with an initial denaturation at 94˚C for 3 min., followed by 30 cycles of a denaturation at 94˚C for 1min, annealing at 55˚C for 1 min, and amplification at 72˚C for 30s with a final elongation at 72˚C for 5 min. The primer pairs only produced amplicons from template DNA from ST631 and each was the expected size (data not shown, and Supplemental Fig. 3). Amplicon assays were applied to 208 clinical isolates from the Northeast US States (ME,

433 NH, MA and CT) and 1140 environmental isolates collected from 2015-2016 from NH and MA.
434 These assays identified all known ST631 clinical isolates with 100% specificity and also
435 identified an additional 7 *tdh*$^{+}$*trh*$^{+}$ clinical isolates (ST631*end* and ST631env positive), and two
436 environmental (ST631end negative and ST631env positive) isolates from our archived collection.
437 Each, with the exception of MAVP-R, was subsequently confirmed to be ST631 by seven-locus
438 MLST (www.pubmlst.org).
439
440 **Examination of *recA* allele and adjacent sequences**
441 The PacBio sequenced genome of MAVP-R, contig 000001 (Accession No.
442 MPPP00000000) that contained the *recA* gene, was annotated using PROKKA1.9 (47). The
443 sequences of *recA* and its surrounding DNA was then compared to the contig containing *recA*
444 region from isolate S130 (AWIW01000000), S134 (AWIS01000000), 090-96 (JFFP01000036)
445 (33) and MAVP-Q (Accession No. MDWT00000000). The map of *recA* region of the five
446 isolates was illustrated using Easyfig (51).
447
448 **Core genome SNP determination and phylogenetic analysis**
449 Whole genome phylogenies were constructed with single nucleotide polymorphisms
450 (SNPs) identified from draft genomes using kSNP3 to produce aligned SNPs in FASTA format
451 (52). A maximum likelihood (ML) tree was then built from the FASTA file using raxMLHPC
452 with model GTRGAMMA and the -f option, and 100 bootstraps (53). Since there were no
453 differences among the clade II ST631 isolates we used a subset representing geographic and
454 temporal span of isolation.

Minimum spanning tree (MST) analysis was built based on core gene SNPs produced from a cluster analysis. The cluster analysis of ST631 was performed using a custom core genome multi-locus sequence type (cgMLST) analysis using RidomSeqSphere+software v3.2.1 (http://www.ridom.de.seqsphere, Ridom GmbH, Münster, Germany) as previously described (31). Briefly, the software first defines a cgMLST scheme using the target definer tool with default settings using the PacBio generated MAVP-Q genome as the reference. Then, five other *V. parahaemolyticus* genomes (BB22OP, CDC_K4557, FDA_R31, RIMD2210633, and UCM-V493) were used for comparison with the reference genome to establish the core and accessory genome genes. Genes that are repeated in more than one copy in any of the six genomes were removed from the analysis. Subsequently, a task template was created that contains both core and accessory genes. Each individual gene locus from MAVP-Q was assigned allele number 1. Then each ST631 isolate genome assembly was queried against the task template, where any locus that differed from the reference genome or any other queried genome was assigned a new allele number. The cgMLST performed a gene-by-gene analysis of all core genes (excluding accessory genes) and identified SNPs within different alleles to establish genetic distance calculations.

Configuration and distribution of VPaIs

The VPaI sequence from the PacBio sequenced genomes of MAVP-Q and MAVP-R were identified by comparison with the published RIMD2210633 VPaI-7 (NC_004605 region between VPA1312 – VPA1395) and $VPaI_{TH3996}$ (AB455531) (16). Identification of the complete MAVP-Q VPaIγ and genomic junctures in chromosome II was done by comparison with the same region of chromosome II in MAVP-R and G149 (which lack an island in this location) using Mauve (54). In a reciprocal manner, the absence of an island in chromosome I in MAVP-Q

and G149 was assessed by comparison with chromosome I of MAVP-R. MAVP-Q VPaIγ (MF066646) and MAVP-R VPaIβ (MF066647) were then extracted as a single contiguous sequence and annotated using Prokka 1.9. Gene content and order of the VPaI elements in MAVP-Q, MAVP-R and RIMD2210633 were then illustrated by Easyfig (51). Roary (55) was then employed to determine homologs among VPaIs based on each island's annotated sequences with identity set at 50%. Identification of the genome locations of VPaIβ in ST1127 isolate MAVP-M (accession number GCA_001023155) and for VPaIγ in AQ4037 (accession number GCA_000182365) (17) was also done using Mauve (54).

To examine the distribution of the VPaIγ in all publicly available draft genomes (https://www.ncbi.nlm.nih.gov/genome/genomes/691, 2016) and genomes from archived regional isolates, whole draft genome sequences were aligned to a 6,118 bp subsequence of the MAVP-Q VPaI with NASP version 1.0.2 (56) (https://pypi.python.org/pypi/nasp/1.0.2, 2017). This subsequence spanned the unique juncture of the four conserved hypothetical proteins (AB831_22090, AB831_22095, AB831_22100, AB831_22105) with the adjacent inserted *tdh* (AB831_22110, c.a. 2549 bp upstream of *ure* cluster)(Supplemental Fig. 1). Percent coverage of the reference sequence was used to determine whether each genome harbored only the four hypothetical proteins, only a *tdh* gene, or the entire module including the fusion of the four genes with *tdh* (Supplemental Fig. 1 and Supplemental Table 3). The sequence type of each genome harboring the fused element characteristic of VPaIγ was then determined using the SRST2 pipeline (48). Where sequencing reads were not available as the input for SRST2, they were simulated from assemblies using an in-house Python script (https://github.com/kpdrees/fasta2reads).

A PCR amplification approach was developed and applied to survey the presence of *tdh* adjacent to the *ure* gene cluster. Primers were designed to conserved sequences of the 3' end of *tdh* (PIHybF8: 5'GCCAACATGGATATAAATAAAAATGA3') and the 5' end of *ureG* (tdhUreGrev5: 5'GACAAAGGTATGCTGCCAAAAGTG3') as determined by gene alignments, which when used together produced a 2631 bp amplicon of the insertion juncture when used with MAVP-Q as a template (Supplemental Fig. 4). Amplification was performed on purified DNA with Accustart enzyme mix, with an initial denaturation at 94˚C for 3 min., followed by 30 cycles of a denaturation at 94˚C for 1 min, annealing at 61˚C for 1min, and amplification at 72˚C for 2.5 min, with a final elongation at 72˚C for 5 min. This amplification was performed in parallel with a diagnostic multiplex PCR amplification of *tdh*, *trh* and *tlh* using published methods (10, 57) to investigate the co-occurrence of VPaIγ with both hemolysin encoding genes in representative isolates of various clinically prevalent sequence types. Amplicons were visualized using a 1.2% agarose gel in TAE buffer (Supplemental Fig. 4).

Nucleotide sequence accession numbers.

The accession number of Pacific Biosciences sequenced genome for MAVP-Q is MDWT00000000, and for MAVP-R is MPPP00000000. The accession number of Illumina sequenced draft genome for G6928 is MPPN00000000, for MA561 is MPPM00000000 and for G149 is MPPO00000000. Detailed information about all other ST631 isolate draft genomes were described previously (31) and are listed in Supplemental Table 1. The accessions for the short reads for the remaining sequenced genomes are listed in Supplemental Table 4. The accession number of VPaIβ from MAVP-R is MF066647 and the accession number of VPaIγ from MAVP-Q is MF066646.

523

524 ACKNOWLEDGEMENTS

525

526 We are grateful for clinical isolates and wish to thank specifically: Jana Ferguson and Tracy
527 Stiles of the Massachusetts Department of Public Health, and M. Hickey and C. Schillaci from
528 the Massachusetts Department of Marine Fisheries; J.K. Kanwit of the Maine Department of
529 Marine Resources and A. Robbins from the Maine Department of Health and Human Services;
530 and Laurn Mank from the Connecticut Department of Public Health Laboratory, and K.
531 DeRosia-Banick, Connecticut Department of Agriculture, Bureau of Aquaculture. Assistance
532 with genome sequencing was provided by W. K. Thomas, and technical assistance provided by J.
533 Lemaire, K. Hartman, C. Hallee, M. Malanga, S. Ilyas, J. Hall, J. Sevigny, M. Dillon, K. Flynn,
534 A. Goupil, J. Means, R. Foxall, E. DaSilva, and M.S. Pankey. Partial funding for this work was
535 provided by the USDA National Institute of Food and Agriculture (Hatch projects NH00574,
536 NH00609 [accession number 233555], and NH00625 [accession number 1004199]). Additional
537 funding was provided by the National Oceanic and Atmospheric Administration College Sea
538 Grant program and grants R/CE-137, R/SSS-2, and R/HCE-3. Support was also provided
539 through the National Institutes of Health (1R03AI081102-01), the National Science Foundation
540 (EPSCoR IIA-1330641), and the National Science Foundation (DBI 1229361 NSF MRI). N.G.-
541 E. was funded through the FDA Foods Science and Research Intramural Program. Feng Xu and
542 Cheryl A. Whistler declare a potential conflict of interest in the form of a pending patent
543 application (U.S. patent application 62/128,764). This is Scientific Contribution Number 2722
544 for the New Hampshire Agricultural Experiment Station.

545

REFERENCES

1. **Hiyoshi H, Kodama T, Iida T, Honda T.** 2010. Contribution of *Vibrio parahaemolyticus* virulence factors to cytotoxicity, enterotoxicity, and lethality in mice. Infect Immun **78:**1772-1780.

2. **Scallan E, Hoekstra RM, Angulo FJ, Tauxe RV, Widdowson M-A, Roy SL, Jones JL, Griffin PM.** 2011. Foodborne illness acquired in the United States—major pathogens. Emerg Infect Dis **17(1):**7-15.

3. **Hazen TH, Pan L, Gu J-D, Sobecky PA.** 2010. The contribution of mobile genetic elements to the evolution and ecology of *Vibrios*. FEMS Microbiol Ecol **74:**485-499.

4. **Hurley CC, Quirke A, Reen FJ, Boyd EF.** 2006. Four genomic islands that mark post-1995 pandemic *Vibrio parahaemolyticus* isolates. BMC Genomics **7:**104 DOI:110.1186/1471-2164-1187-1104.

5. **Boyd EF, Cohen AL, Naughton LM, Ussery DW, Binnewies TT, Stine OC, Parent MA.** 2008. Molecular analysis of the emergence of pandemic *Vibrio parahaemolyticus*. BMC Microbiol **8:**110.

6. **Kishishita M, Matsuoka N, Kumagai K, Yamasaki S, Takeda Y, Nishibuchi M.** 1992. Sequence variation in the thermostable direct hemolysin-related hemolysin (*trh*) gene of *Vibrio parahaemolyticus*. Appl Environ Microbiol **58:**2449-2457.

7. **Honda T, Ni Y, Miwatani T, Adachi T, Kim J.** 1992. The thermostable direct hemolysin of *Vibrio parahaemolyticus* is a pore-forming toxin. Can J Microbiol **38:**1175-1180.

8. **Park K-S, Ono T, Rokuda M, Jang M-H, Iida T, Honda T.** 2004. Cytotoxicity and enterotoxicity of the thermostable direct hemolysin-deletion mutants of *Vibrio parahaemolyticus*. Microbiol Immunol **48:**313-318.

9. **Shirai H, Ito H, Hirayama T, Nakamoto Y, Nakabayashi N, Kumagai K, Takeda Y, Nishibuchi M.** 1990. Molecular epidemiologic evidence for association of thermostable direct hemolysin (TDH) and TDH-related hemolysin of *Vibrio parahaemolyticus* with gastroenteritis. Infect Immun **58:**3568-3573.

10. **Panicker G, Call DR, Krug MJ, Bej AK.** 2004. Detection of pathogenic *Vibrio* spp. in shellfish by using multiplex PCR and DNA microarrays. Appl Environ Microbiol **70:**7436-7444.

11. **Nishibuchi M, Kaper JB.** 1995. Thermostable direct hemolysin gene of *Vibrio parahaemolyticus*: a virulence gene acquired by a marine bacterium. Infect Immun **63:**2093.

12. **Park K-S, Ono T, Rokuda M, Jang M-H, Okada K, Iida T, Honda T.** 2004. Functional characterization of two type III secretion systems of *Vibrio parahaemolyticus*. Infect Immun **72:**6659-6665.

13. **Broberg CA, Calder TJ, Orth K.** 2011. *Vibrio parahaemolyticus* cell biology and pathogenicity determinants. Microb Infect **13:**992-1001.

14. **Zhang L, Orth K.** 2013. Virulence determinants for *Vibrio parahaemolyticus* infection. Curr Opin Microbiol **16:**70-77.

15. **Makino K, Oshima K, Kurokawa K, Yokoyama K, Uda T, Tagomori K, Iijima Y, Najima M, Nakano M, Yamashita A.** 2003. Genome sequence of *Vibrio*

parahaemolyticus: a pathogenic mechanism distinct from that of *V. cholerae*. The Lancet **361:**743-749.

16. **Okada N, Iida T, Park K-S, Goto N, Yasunaga T, Hiyoshi H, Matsuda S, Kodama T, Honda T.** 2009. Identification and characterization of a novel type III secretion system in trh-positive *Vibrio parahaemolyticus* strain TH3996 reveal genetic lineage and diversity of pathogenic machinery beyond the species level. Infect Immun **77:**904-913.

17. **Chen Y, Stine OC, Badger JH, Gil AI, Nair GB, Nishibuchi M, Fouts DE.** 2011. Comparative genomic analysis of *Vibrio parahaemolyticus*: serotype conversion and virulence. BMC Genomics **12:**1.

18. **Zhou X, Gewurz BE, Ritchie JM, Takasaki K, Greenfeld H, Kieff E, Davis BM, Waldor MK.** 2013. *vopZ* A *Vibrio parahaemolyticus* T3SS effector mediates pathogenesis by independently enabling intestinal colonization and inhibiting TAK1 activation. Cell Reports **3:**1690-1702.

19. **Hubbard TP, Chao MC, Abel S, Blondel CJ, zur Wiesch PA, Zhou X, Davis BM, Waldor MK.** 2016. Genetic analysis of *Vibrio parahaemolyticus* intestinal colonization. Proc Nat Acad Sci USA **113:**6283-6288.

20. **Ronholm J, Petronella N, Leung CC, Pightling A, Banerjee S.** 2016. Genomic Features of Environmental and Clinical *Vibrio parahaemolyticus* Isolates Lacking Recognized Virulence Factors Are Dissimilar. Appl Environ Microbiol **82:**1102-1113.

21. **Xu F, Ilyas S, Hall JA, Jones SH, Cooper VS, Whistler CA.** 2015. Genetic characterization of clinical and environmental *Vibrio parahaemolyticus* from the Northeast USA reveals emerging resident and non-indigenous pathogen lineages. Name: Front Microbiol **6:**272.

22. **Banerjee SK, Kearney AK, Nadon CA, Peterson C-L, Tyler K, Bakouche L, Clark CG, Hoang L, Gilmour MW, Farber JM.** 2014. Phenotypic and genotypic characterization of Canadian clinical isolates of *Vibrio parahaemolyticus* collected from 2000 to 2009. J Clin Microbiol **52:**1081-1088.

23. **Turner JW, Paranjpye RN, Landis ED, Biryukov SV, González-Escalona N, Nilsson WB, Strom MS.** 2013. Population structure of clinical and environmental *Vibrio parahaemolyticus* from the Pacific Northwest coast of the United States. PLoS ONE **8(2):**e55726

24. **Jones JL, Lüdeke CH, Bowers JC, Garrett N, Fischer M, Parsons MB, Bopp CA, DePaola A.** 2012. Biochemical, serological, and virulence characterization of clinical and oyster *Vibrio parahaemolyticus* isolates. J Clin Microbiol **50(7):**2343-2352.

25. **DePaola A, Ulaszek J, Kaysner CA, Tenge BJ, Nordstrom JL, Wells J, Puhr N, Gendel SM.** 2003. Molecular, serological, and virulence characteristics of *Vibrio parahaemolyticus* isolated from environmental, food, and clinical sources in North America and Asia. Appl Environ Microbiol **69:**3999-4005.

26. **Haendiges J, Timme R, Allard MW, Myers RA, Brown EW, Gonzalez-Escalona N.** 2015. Characterization of *Vibrio parahaemolyticus* clinical strains from Maryland (2012–2013) and comparisons to a locally and globally diverse *V. parahaemolyticus* strains by whole-genome sequence analysis. Front Microbiol **6**.125

27. **Ellis CN, Schuster BM, Striplin MJ, Jones SH, Whistler CA, Cooper VS.** 2012. Influence of seasonality on the genetic diversity of *Vibrio parahaemolyticus* in New Hampshire shellfish waters as determined by multilocus sequence analysis. Appl Environ Microbiol **78:**3778-3782.

635 28. **Nair GB, Ramamurthy T, Bhattacharya SK, Dutta B, Takeda Y, Sack DA.** 2007.
636 Global dissemination of *Vibrio parahaemolyticus* serotype O3: K6 and its serovariants.
637 Clin Microbiol Rev **20:**39-48.
638 29. **Martinez-Urtaza J, Baker-Austin C, Jones JL, Newton AE, Gonzalez-Aviles GD,**
639 **DePaola A.** 2013. Spread of Pacific Northwest *Vibrio parahaemolyticus* strain. N Engl J
640 Med **369:**1573-1574.
641 30. **Newton AE, Garrett N, Stroika SG, Halpin JL, Turnsek M, Mody RK, Division of**
642 **Foodborne W, Environmental D.** 2014. Notes from the field: Increase in *Vibrio*
643 *parahaemolyticus* infections associated with consumption of Atlantic coast shellfish—
644 2013. MMWR Morb Mortal Wkly Rep **63:**335-336.
645 31. **Xu F, Gonzalez-Escalona N, Haendiges J, Myers RA, Ferguson J, Stiles T, Hickey E,**
646 **Moore M, Hickey JM, Schillaci C.** 2017. Sequence type 631 *Vibrio parahaemolyticus*,
647 an emerging foodborne pathogen in North America. J Clin Microbiol **55:**645-648.
648 32. **Lüdeke CH, Gonzalez-Escalona N, Fischer M, Jones JL.** 2015. Examination of
649 clinical and environmental *Vibrio parahaemolyticus* isolates by multi-locus sequence
650 typing (MLST) and multiple-locus variable-number tandem-repeat analysis (MLVA).
651 Frontiers in microbiology **6**.564
652 33. **González-Escalona N, Gavilan RG, Brown EW, Martinez-Urtaza J.** 2015.
653 Transoceanic spreading of pathogenic strains of *Vibrio parahaemolyticus* with distinctive
654 genetic signatures in the recA gene. PloS one **10:**e0117485.
655 34. **Park K-S, Suthienkul O, Kozawa J, Yamaichi Y, Yamamoto K, Honda T.** 1998.
656 Close proximity of the *tdh, trh* and *ure* genes on the chromosome of *Vibrio*
657 *parahaemolyticus*. Microbiology **144:**2517-2523.

658 35. **Johnson C, Flowers A, Young V, Gonzalez-Escalona N, DePaola A, Noriea III N,**
659 **Grimes D.** 2009. Genetic relatedness among *tdh*+ and *trh*+ *Vibrio parahaemolyticus*
660 cultured from Gulf of Mexico oysters (Crassostrea virginica) and surrounding water and
661 sediment. Microb Ecol **57:**437-443.
662 36. **González-Escalona N, Martinez-Urtaza J, Romero J, Espejo RT, Jaykus L-A,**
663 **DePaola A.** 2008. Determination of molecular phylogenetics of *Vibrio parahaemolyticus*
664 strains by multilocus sequence typing. J Bacteriol **190:**2831-2840.
665 37. **Ellingsen BA, Olsen JS, Granum PE, Rorvik LM, González-Escalona N.** 2013.
666 Genetic characterization of trh positive Vibrio spp. isolated from Norway. Front Cell
667 Infect Microbiol **3:**107.
668 38. **Chen Y, Dai J, Morris JG, Johnson JA.** 2010. Genetic analysis of the capsule
669 polysaccharide (K antigen) and exopolysaccharide genes in pandemic *Vibrio*
670 *parahaemolyticus* O3: K6. BMC Microbiol **10:**1.
671 39. **Meibom KL, Blokesch M, Dolganov NA, Wu C-Y, Schoolnik GK.** 2005. Chitin
672 induces natural competence in *Vibrio cholerae*. Science **310:**1824-1827.
673 40. **Takemura AF, Chien DM, Polz MF.** 2014. Associations and dynamics of *Vibrionaceae*
674 in the environment, from the genus to the population level. Front Microbiol 5**:**38.
675 41. **Lovell CR.** 2017. Ecological fitness and virulence features of *Vibrio parahaemolyticus* in
676 estuarine environments. Appl Microbiol Biotechnol 101:1781-1794.
677 42. **Johnson CN.** 2013. Fitness factors in vibrios: a mini-review. Microb Ecol **65:**826-851.
678 43. **Matz C, Nouri B, McCarter L, Martinez-Urtaza J.** 2011. Acquired type III secretion
679 system determines environmental fitness of epidemic *Vibrio parahaemolyticus* in the
680 interaction with bacterivorous protists. PloS one **6:**e20275.

44. **Nishibuchi M, Kaper JB.** 1985. Nucleotide sequence of the thermostable direct hemolysin gene of *Vibrio parahaemolyticus*. J Bacteriol **162:**558-564.

45. **Baym M, Kryazhimskiy S, Lieberman TD, Chung H, Desai MM, Kishony R.** 2015. Inexpensive multiplexed library preparation for megabase-sized genomes. PloS one **10:**e0128036.

46. **Tritt A, Eisen JA, Facciotti MT, Darling AE.** 2012. A5. An integrated pipeline for *de novo* assembly of microbial genomes. PLoS ONE **7:**e42304.

47. **Seemann T.** 2014. Prokka: rapid prokaryotic genome annotation. Bioinformatics**. 30:**2068-9

48. **Inouye M, Conway TC, Zobel J, Holt KE.** 2012. Short read sequence typing (SRST): multi-locus sequence types from short reads. BMC Genomics **13:**338.

49. **Walker BJ, Abeel T, Shea T, Priest M, Abouelliel A, Sakthikumar S, Cuomo CA, Zeng Q, Wortman J, Young SK.** 2014. Pilon: an integrated tool for comprehensive microbial variant detection and genome assembly improvement. PloS one **9:**e112963.

50. **Camacho C, Coulouris G, Avagyan V, Ma N, Papadopoulos J, Bealer K, Madden TL.** 2009. BLAST+: architecture and applications. BMC Bioinformatics **10:**421.

51. **Sullivan MJ, Petty NK, Beatson SA.** 2011. Easyfig: a genome comparison visualizer. Bioinformatics **27:**1009-1010.

52. **Gardner SN, Slezak T, Hall BG.** 2015. kSNP3. 0: SNP detection and phylogenetic analysis of genomes without genome alignment or reference genome. Bioinformatics **31:**2877-8.

53. **Stamatakis A.** 2006. RAxML-VI-HPC: maximum likelihood-based phylogenetic analyses with thousands of taxa and mixed models. Bioinformatics **22:**2688-2690.

54. **Darling AC, Mau B, Blattner FR, Perna NT.** 2004. Mauve: multiple alignment of conserved genomic sequence with rearrangements. Genome Res **14:**1394-1403.

55. **Page AJ, Cummins CA, Hunt M, Wong VK, Reuter S, Holden MT, Fookes M, Falush D, Keane JA, Parkhill J.** 2015. Roary: rapid large-scale prokaryote pan genome analysis. Bioinformatics **31:**3691-3693.

56. **Sahl JW, Lemmer D, Travis J, Schupp J, Gillece J, Aziz M, Driebe E, Drees K, Hicks N, Williamson C.** 2016. The Northern Arizona SNP Pipeline (NASP): accurate, flexible, and rapid identification of SNPs in WGS datasets. Microb Genom. **2**:e000074

57. **Whistler CA, Hall JA, Xu F, Ilyas S, Siwakoti P, Cooper VS, Jones SH.** 2015. Use of Whole-Genome Phylogeny and Comparisons for Development of a Multiplex PCR Assay To Identify Sequence Type 36 *Vibrio parahaemolyticus*. J Clin Microbiol **53:**1864-1872.

58. **Jolley KA, Chan M-S, Maiden MC.** 2004. mlstdbNet–distributed multi-locus sequence typing (MLST) databases. BMC Bioinformatics **5:**86.

59. **Alikhan N-F, Petty NK, Zakour NLB, Beatson SA.** 2011. BLAST Ring Image Generator (BRIG): simple prokaryote genome comparisons. BMC Genomics **12:**402

Table 1: Clinical and environmental prevalence of emergent Northeast US *V. parahaemolyticus* lineages with associated virulence features.

Sequence type[a]	**Northeast US States**[b]		**MLST Database**[c]		**Hemolysin genotype**	**VPaI type**[d]
	Clinical	Environmental	Clinical	Environmental		
3	2	0	217	33	*tdh*$^+$	α
36	91	1	58	5	*tdh*$^+$*trh*$^+$	γ
631	24	0	12	0	*tdh*$^+$*trh*$^+$	γ
	1[e]	2	0	0	*trh*$^+$	β
	0	1	0	0	neither	absent
43	5	0	17	4	*tdh*$^+$*trh*$^+$	γ
636	4	0	2	0	*tdh*$^+$*trh*$^+$	γ
1127	4	0	0	0	*trh*$^+$	β
110	3	0	0	1	*tdh*$^+$*trh*$^+$	γ
34/324	2	2	4	19	*tdh*$^+$*trh*$^+$	γ
674	0	4	1	20	*tdh*$^+$*trh*$^+$	γ
	1	0	0	0	neither	absent
308	2	0	0	2	*tdh*$^+$*trh*$^+$	γ
12	2	0	0	4	*trh*$^+$	β
162	2	0	1	1	neither	absent
194	2	0	1	0	neither	absent
809	2	0	0	1	*trh*$^+$	β
1716	2	0	0	0	*trh*$^+$	β
1123	1	1	0	0	*trh*$^+$	β
8	1	0	13	5	*trh*$^+$	β
23	1	0	0	3	*tdh*$^+$*trh*$^+$	γ
749	1	0	1	0	*tdh*$^+$*trh*$^+$	γ
1295	1	0	0	1	neither	absent
134	1	0	1	0	neither	absent
741	1	0	0	1	neither	absent
98	1	0	0	1	*trh*$^+$	β
1205	1	0	0	1	neither	absent
1561	1	0	0	0	neither	absent
1717	1	0	0	0	neither	absent
1725	1	0	0	0	*tdh*$^+$	α

[a] Some clinical isolates had insufficient sequencing coverage to determine sequence type and included eight *tdh*$^+$*trh*$^+$ isolates, one *tdh*$^+$ isolate, four *trh*$^+$ isolates, and 11 isolates without hemolysins, some of which were from wound infections. Two wound infection isolates lacking hemolysins were of known sequence types and are not listed above.

[b]Data generated from all available gastric infection clinical and environmental isolates four reporting Northeast US States including ME, NH, MA, and CT between 2010 and 2016.

[c]http://pubmlst.org/vparahaemolyticus, 2017 (36, 58)

[d]Presence of the VPaIγ architecture was determined by PacBio genome sequencing of isolate MAVP-Q and MAVP-26, whereas for other isolates, identification of VPaI type was determined through illumina genome sequencing, PCR amplification and Sanger sequencing.

[e]This single isolate harbors a *recA* allele (allele 21) typical of ST631 fused to allele 107 through an insertion event, generating a hybrid allele previously described (33).

737 Figure 1. Schematic of a horizontally acquired insertion in the *recA*-encoding region of MAVP-R.
738 Sequences of the *recA* gene and flanking region from MAVP-Q (reference ST631 genome),
739 MAVP-R, Asia-derived isolates S130/S134 and Peru-derived isolate 090-96 were extracted and
740 aligned. Open reading frames designated with arrows and illustrated by representative colors to
741 highlight homologous and unique genes. The % similarity between homologs is illustrated by
742 grey bars.
743
744 Figure 2. Phylogenetic relationships of *V. parahaemolyticus* lineages and identification of
745 distinct ST631 clades. An ML phylogeny of representative *V. parahaemolyticus* genomes of
746 clinical isolates causing two or more infections was built on whole genome SNPs identified by
747 reference-free comparisons as described in the methods. The branch length represents the
748 number of nucleotide substitutions per site. Numbers at nodes represent percent bootstrap
749 support where unlabeled nodes had bootstraps of less than 70.
750
751 Figure 3. Minimum spanning tree relationships among clade I and clade II ST631. A cgMLST
752 core gene-by-gene analysis (excluding accessory genes) was performed and SNPs were
753 identified within different alleles. The numbers above the connected lines (not to scale) represent
754 SNP differences. The isolates are colored based on different hemolysin genotypes as labeled.
755
756 Figure 4. Comparisons of the pathogenicity islands containing hemolysins and T3SS2.
757 Sequences of VPaI were extracted from select genomes and aligned. VPaIα was derived from
758 ST3 strain RIMD2210633, VPaIγ was derived from ST631 clade II isolate MAVP-Q, and VPaIβ
759 was derived from ST631 clade I isolate MAVP-R. ORFs are depicted in defined colors and

760 similarities (≥75%) among ORFs are illustrated in grey blocks. Homologs between VPaIα and
761 VPaIβ/γ (50□75% identity) are named and listed in Supplemental Table 2.
762
763 Figure 5. Distribution of VPaIγ in emergent pathogen lineages. The presence of *tdh*, *trh* and
764 VPaIγ along with positive control *tlh* was determined by PCR amplification using gene-specific
765 primers and visualized on a 1.2% agarose gel. The order from left to right is 1kb+ ladder, ST3
766 (MAVP-C), ST36 (MAVP-26), ST631 CII (clade II isolate MAVP-Q), ST631 CI (clade I
767 isolates MAVP-R and G149), ST43 (MAVP-71), ST636 (MAVP-50), ST1127 (MAVP-M),
768 ST110 (MAVP-46), ST34 (CTVP19C), ST324 (MAVP-14), and ST674 (CT4291, MAVP21).
769 The corresponding sizes of the ladder fragments are as labeled to the left and the identity of the
770 amplicons listed to the right of the gel image.

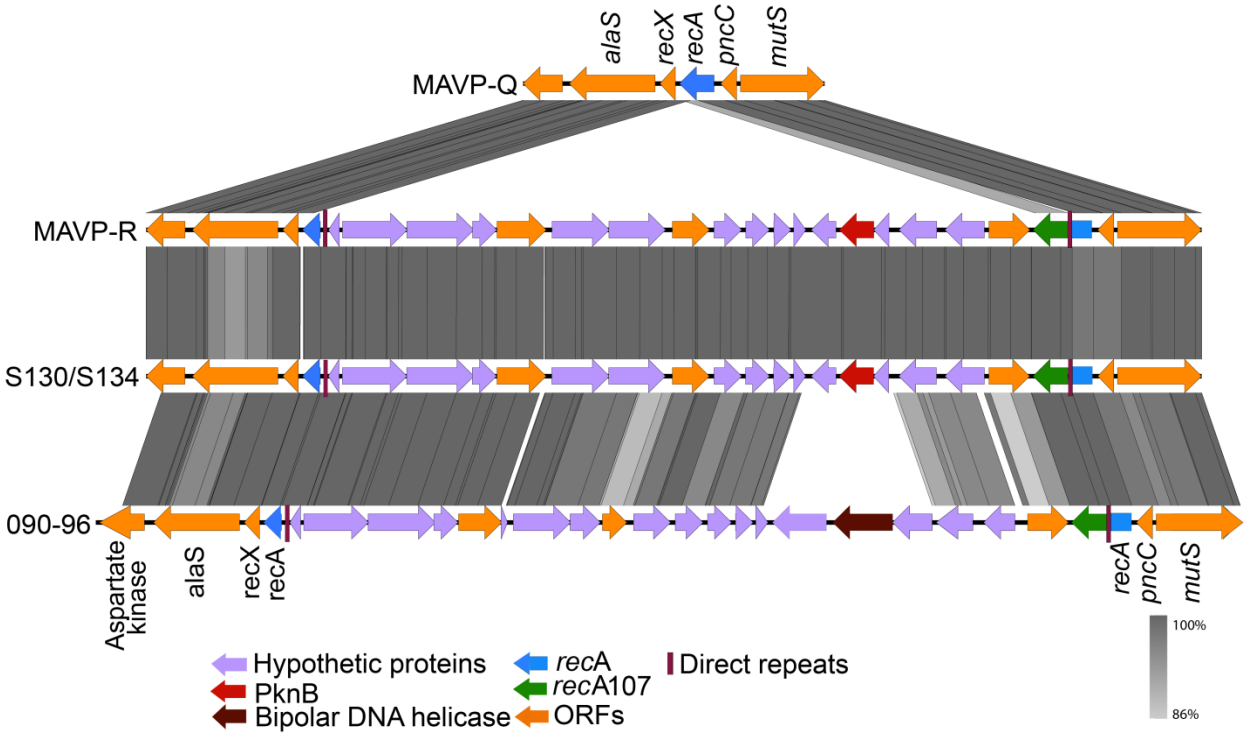

Figure 1. Schematic of a horizontally acquired insertion in the *recA*-encoding region of MAVP-R. Sequences of the *recA* gene and flanking region from MAVP-Q (reference ST631 genome), MAVP-R, Asia-derived isolates S130/S134 and Peru-derived isolate 090-96 were extracted and aligned. Open reading frames designated with arrows and illustrated by representative colors to highlight homologous and unique genes. The % similarity between homologs is illustrated by grey bars.

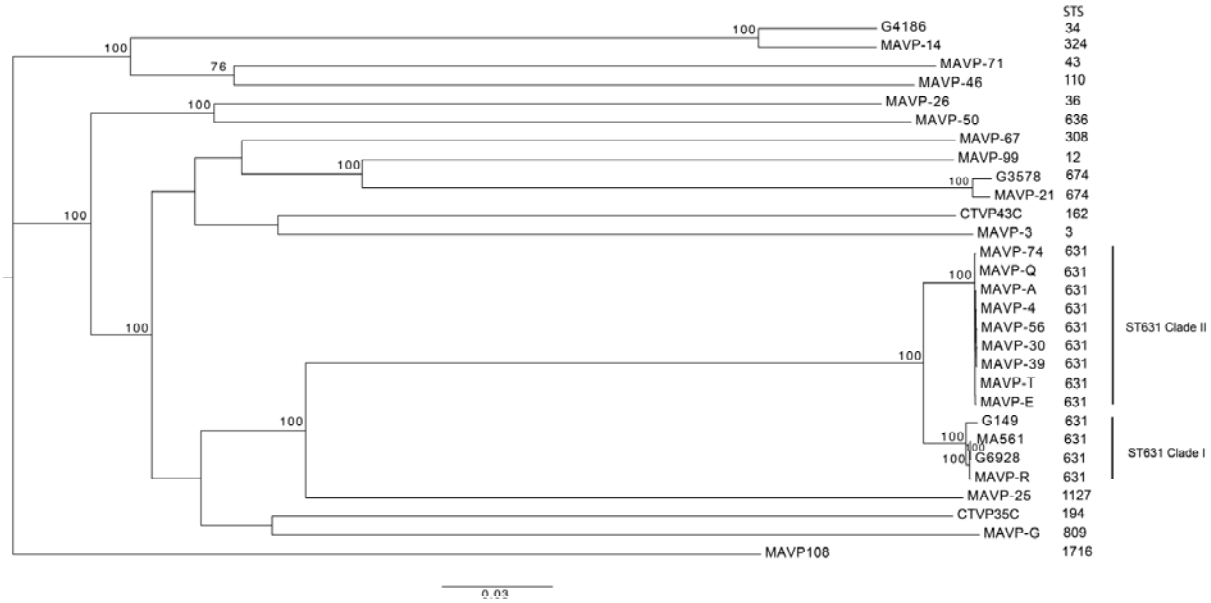

Figure 2. Phylogenetic relationships of *V. parahaemolyticus* lineages and identification of distinct ST631 clades. An ML phylogeny of representative *V. parahaemolyticus* genomes of clinical strains causing two or more infections was built on whole genome SNPs identified by reference-free comparisons as described in the methods, The branch length represents the number of nucleotide substitutions per site. Numbers at nodes represent percent bootstrap support where unlabeled nodes had bootstraps of less than 70.

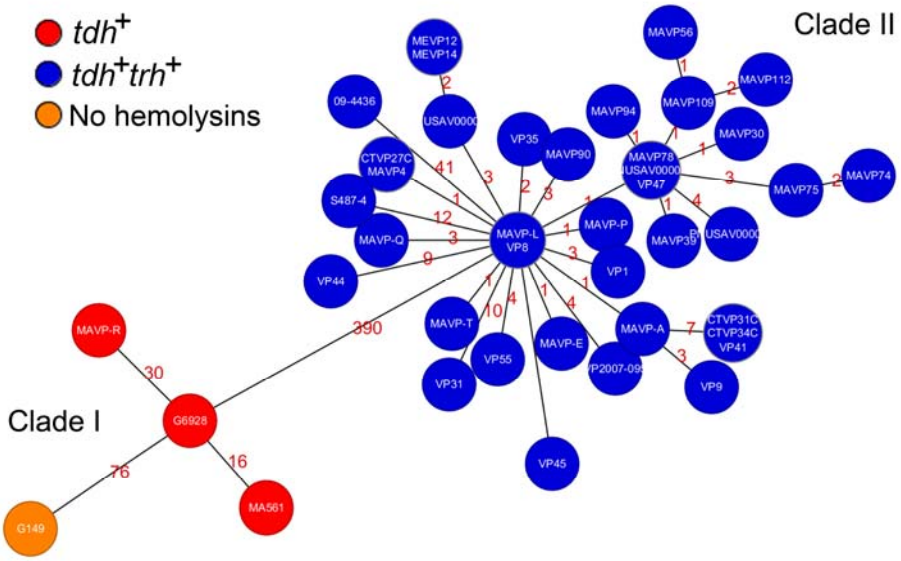

Figure 3. Minimum spanning tree relationships among clade I and clade II ST631. A core gene-by-gene analysis (excluding accessory genes) was performed and SNPs were identified within different alleles. The numbers above the connected lines (not to scale) represent SNP differences. The isolates are colored based on different hemolysin genotypes as labeled.

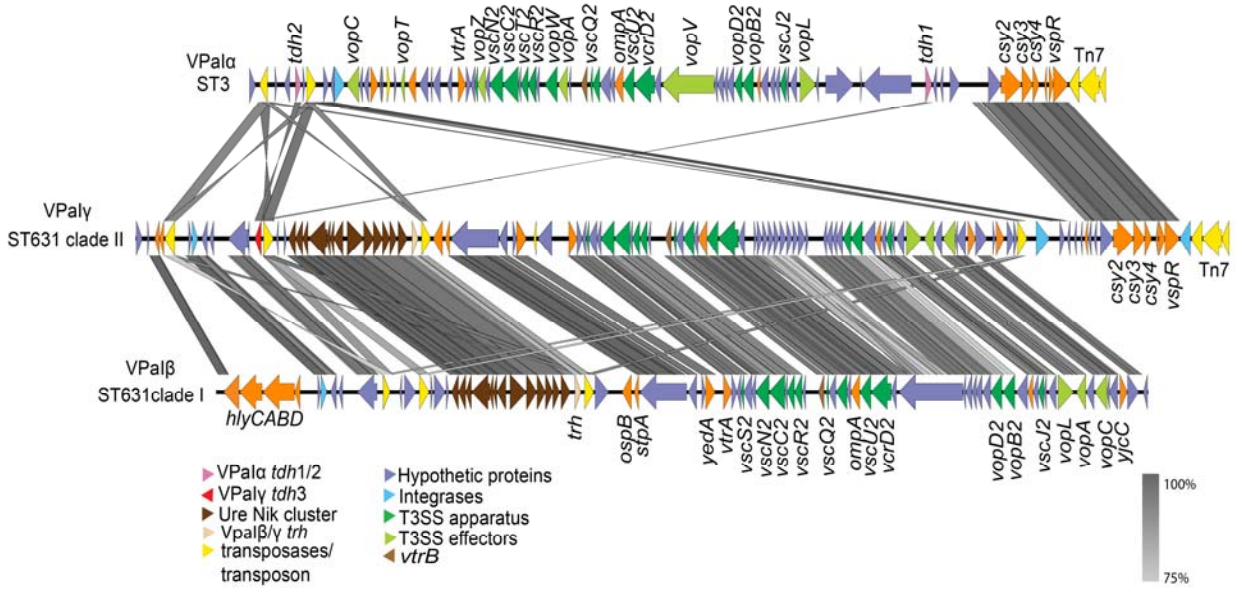

Figure 4. Comparisons of the pathogenicity islands containing hemolysins and T3SS2. Sequences of VPaI were extracted from select genomes and aligned. VPaIα was derived from ST3 strain RIMD2210633, VPaIγ was derived from ST631 clade II isolate MAVP-Q, and VPaIβ was derived from ST631 clade I isolate MAVP-R. ORFs are depicted in defined colors and similarities (≥75%) among ORFs are illustrated in grey blocks. omologs between VPaIα and VPaIβ/γ (50□75% identity) are named and listed in supplemenatal table 2.

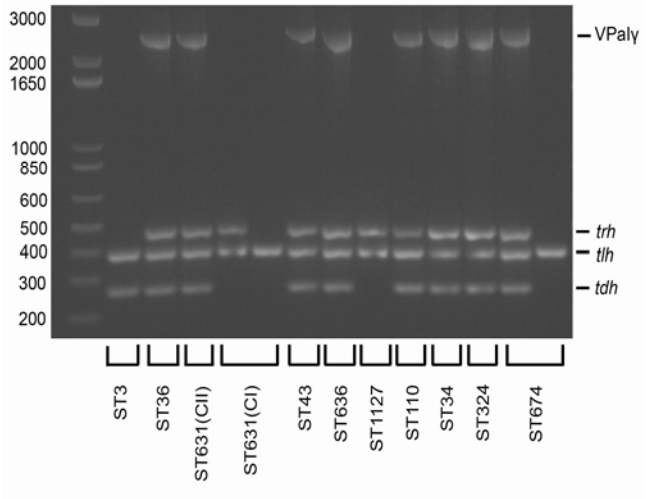

Figure 5. Distribution of VPaIγ in emergent pathogen lineages. The presence of *tdh*, *trh* and VPaIγ along with positive control *tlh* was determined by PCR amplification using gene-specific primers and visualized on a 1.2% agarose gel. The order from left to right is 1kb+ ladder, ST3 (MAVP-C), ST36 (MAVP-26), ST631 CII (clade II isolate MAVP-Q), ST631 CI (clade I isolates MAVP-R and G149), ST43 (MAVP-71), ST636 (MAVP-50), ST1127 (MAVP-M), ST110 (MAVP-46), ST34 (CTVP19C), ST324 (MAVP-14), and ST674 (CT4291, MAVP21). The corresponding sizes of the ladder fragments are as labeled to the left and the identity of the amplicons listed to the right of the gel image.